Role of Zonal Flow Predator-Prey Oscillations in Triggering the Transition to H-Mode Confinement

L. Schmitz,[1] L. Zeng,[1] T. L. Rhodes,[1] J. C. Hillesheim,[1] E. J. Doyle,[1] R. J. Groebner,[2] W. A. Peebles,[1] K. H. Burrell,[2] and G. Wang[1]

[1]*University of California-Los Angeles, Los Angeles, California 90095, USA*
[2]*General Atomics, Post Office Box 85608, San Diego, California 92186-5608, USA*

(Received 23 August 2011; published 12 April 2012)

Direct evidence of zonal flow (ZF) predator-prey oscillations and the synergistic roles of ZF- and equilibrium $\boldsymbol{E} \times \boldsymbol{B}$ flow shear in triggering the low- to high-confinement (L- to H-mode) transition in the DIII-D tokamak is presented. Periodic turbulence suppression is first observed in a narrow layer at and just inside the separatrix when the shearing rate transiently exceeds the turbulence decorrelation rate. The final transition to H mode with sustained turbulence and transport reduction is controlled by equilibrium $\boldsymbol{E} \times \boldsymbol{B}$ shear due to the increasing ion pressure gradient.

DOI: 10.1103/PhysRevLett.108.155002 PACS numbers: 52.35.Ra, 05.45.−a, 52.25.Fi, 52.55.Fa

Zonal flows (ZFs) are ubiquitous in fluid turbulence, for example, in planetary atmospheres [1], and the terrestrial jet stream, and are of general interest in turbulence self-organization across different scales. Over the last decade, it has been recognized that spontaneously generated ZFs may also play an important role for turbulence or transport self-regulation in magnetically confined plasmas [2,3]. Considerable attention has focused on their potential role as a trigger mechanism for the transition from low- to high-confinement regimes (L- to H-mode transition [4–6]) in toroidal fusion plasmas [7–10], reducing edge plasma turbulence (and transport) possibly in combination with equilibrium $\boldsymbol{E} \times \boldsymbol{B}$ flow shear [5]. Understanding the transition dynamics and power threshold scaling is important to assess auxiliary heating requirements for future burning plasma experiments. A predator-prey model of the L-H transition has been proposed, including the interaction of turbulence, time-dependent zonal flows driven by the Reynolds stress, and equilibrium $\boldsymbol{E} \times \boldsymbol{B}$ shear due to the radial ion pressure gradient [11]. In this model, the ZF and equilibrium flow shear are two competing predators interacting with drift wave turbulence (prey). $\boldsymbol{E} \times \boldsymbol{B}$ flow velocity fluctuations potentially consistent with ZFs, preceding the L-H transition have been observed recently in several experiments [9,10,12–14]. The Reynolds stress thought to generate ZFs has been measured directly in improved Ohmic confinement discharges [15]. Transient phases of "H-mode-like" behavior with increased flow and reduced turbulence have been observed in the NSTX tokamak preceding the LH transition [12], and ZFs are considered a likely explanation. In the ASDEX-U tokamak, a periodic modulation of flow and turbulence level, with the characteristics of a limit cycle oscillation at the geodesic acoustic mode (GAM) frequency, has been observed preceding the LH transition in low density plasmas [13].

In this Letter we present direct evidence of (i) predator-prey oscillations with characteristic signatures of a low frequency ZF (with a frequency much below the GAM frequency) preceding the L-H transition; (ii) periodic turbulence suppression *starting* at and just inside the separatrix when the local ZF $\boldsymbol{E} \times \boldsymbol{B}$ shearing rate transiently exceeds the turbulence decorrelation rate; (iii) the importance of the radial structure of the ZF flow layer (double shear layer) in establishing the H-mode edge transport barrier, and (iv) equilibrium shear resulting from the increasing ion pressure gradient controlling the final L-H transition. A so-called dithering L-H transition with input power near the L-H transition threshold is studied here as it allows the investigation of the transition dynamics on an expanded time scale.

Multichannel Doppler backscattering on DIII-D (DBS) [16,17]) provides simultaneous density fluctuation and flow data with high temporal (1 μs) and radial (0.4 cm) resolution across a radius range $0.65 \leq r/a \leq 1.05$ in the L mode and $0.8 \leq r/a \leq 1.05$ in the H mode. DBS utilizes diagnostic microwave beams focused onto the measurement (cutoff layer) radius (spot size $2W_0 \sim 4.5$ cm, where W_0 is the $1/e$ half width of the beam power) launched at an oblique angle to the magnetic flux surfaces at two toroidal locations (toroidal angles $\phi = 60°, 240°$). The diagnostic setup and typical probing radii are shown in Figs. 2(h) and 2(j). Because of refraction, the microwave beam bends predominantly in the poloidal direction. Backscattering by plasma density fluctuations occurs preferentially near the cutoff layer [17], according to the selection rules $k_S = -k_I = k_\theta/2$ and $\omega_S = \omega_I + v_t k_\theta$, where the indices I and S denote the incident and backscattered wave, v_t is the poloidal turbulence advection velocity, and k_θ is the resonant poloidal density fluctuation wave number. The backscattered signal amplitude is proportional to the density fluctuation amplitude $\tilde{n}(k_\theta)$. The probed wave number k_θ, and the probed major radius R are obtained using ray tracing based on high time resolution (25 μs) electron density profiles from profile reflectometry.

The time-resolved $\boldsymbol{E} \times \boldsymbol{B}$ velocity is obtained from the instantaneous Doppler shift, $f_D = (\omega_S - \omega_I)/2\pi = v_\perp k_\theta/(2\pi)$, with $v_\perp = v_{E\times B} + v_{\rm ph}$. Neglecting the contribution of the fluctuation phase velocity $v_{\rm ph}$, (estimated to be much smaller than the electron and ion diamagnetic velocities by linear stability calculations for similar plasmas [18]), one obtains $v_{E\times B} \approx 2\pi f_D/k_\theta$.

Figure 1(a) shows the time history of the $\boldsymbol{E} \times \boldsymbol{B}$ velocity $v_{E\times B}$ across the plasma edge (measured by an 8-channel DBS system) in a dithering L-H transition, induced by stepping up the (co-injected) neutral beam power from $P_{\rm inj} = 2.8$ MW to 4.5 MW, a value just above the H-mode transition power threshold (at a toroidal magnetic field $B_\phi = 2$ T and plasma current $I_p = 1.1$ MA), The core plasma (line density $\bar{n} = 2.7 \times 10^{19}$ m^{-3}) is corotating, and in the L mode the radial electric field $E_r \approx v_\phi B_\theta/B^2$ and the poloidal projection of the $\boldsymbol{E} \times \boldsymbol{B}$ velocity shown here are positive except for a narrow radial edge layer a few cm inside the separatrix, where the contribution of the ion pressure gradient to E_r produces weak intermittent negative flow. The normalized edge density fluctuation level $\tilde{n}/n$ peaks near/outside the separatrix [Fig. 1(b)]. $\tilde{n}/n$ is measured by DBS at a wave number $k_\theta \sim 2.7$ cm^{-1}, $\Delta k_\theta/k_\theta \approx 0.3$, and $k_\theta \rho_s \sim 0.4$. This wave number range overlaps with the upper wave number range detected by beam emission spectroscopy (BES) in DIII-D and corresponds to the poloidal wavenumber range where the maximum growth rate of the ion temperature gradient mode [ITG], is expected. In addition, resistive ballooning modes (RBM) may be active just inside the separatrix. The radiative instability, thought to be responsible for limit cycle oscillations in earlier DIII-D experiments with a higher triangularity plasma with lower x-point height [8], is not likely to be present here due to the higher NBI heating power (2.8 vs 0.3 MW) and edge electron temperature, and low $Z_{\rm eff} \approx 1.6$. Because of backscattering, DBS intrinsically detects modes with $k_r \approx 0$. At $t \sim 1271$ ms, a strong, periodic limit cycle oscillation (LCO) oscillation in the $\boldsymbol{E} \times \boldsymbol{B}$ velocity starts to develop in a 2–3 cm wide layer at and just inside the separatrix. Starting at $t_0 \sim 1271.7$ ms, density fluctuations are periodically reduced in the region 2.25 m $< R <$ 2.28 m, concomitantly with a sharp reduction in the D_α recycling light [Fig. 1(c)]. Edge confinement starts to improve during the oscillatory phase, as evidenced by the changing rate of increase of the line density [Fig. 1(d)] and edge electron temperature [Fig. 1(e)]. The frequency of the $\boldsymbol{E} \times \boldsymbol{B}$ flow oscillation decreases gradually from 2.5 to 1.7 kHz. About 15 ms after LCO onset, after a final D_α transient, the transition to sustained H-mode takes place, characterized by a strong, steady $\boldsymbol{E} \times \boldsymbol{B}$ flow layer with $E_r \sim -\nabla p_i/en$, where ∇p_i is the ion pressure gradient and n is the plasma density. An expanded time history reveals that the $\boldsymbol{E} \times \boldsymbol{B}$ velocity oscillations [Fig. 2(a)] at the separatrix lag the density fluctuation amplitude [Fig. 2(b)] by about 90°, as confirmed by the cross-correlation coefficient [Fig. 2(d)]. This phase lag is consistent with the predator-prey model of the L-H transition advocated previously [11]. ZFs are driven once density fluctuations reach sufficient amplitude; in turn, ZF shear is thought to quench fluctuations. The time delay between the peak fluctuation amplitude (and, presumably, peak radial particle transport flux) and the peak divertor recycling (D_α) light [Fig. 2(c)] is found to be ~120–140 μs, consistent with an estimated plasma loss time due to parallel scrape-off layer (SOL) flow $0.5 q_{95} R/0.3 c_s \approx 140$–$180$ μs (the edge safety factor is $q_{95} \sim 4.1$ and an estimated SOL parallel flow speed of $0.3 c_s$ with $c_s = [(kT_e + kT_i)/m_i]^{1/2}$ is used here).

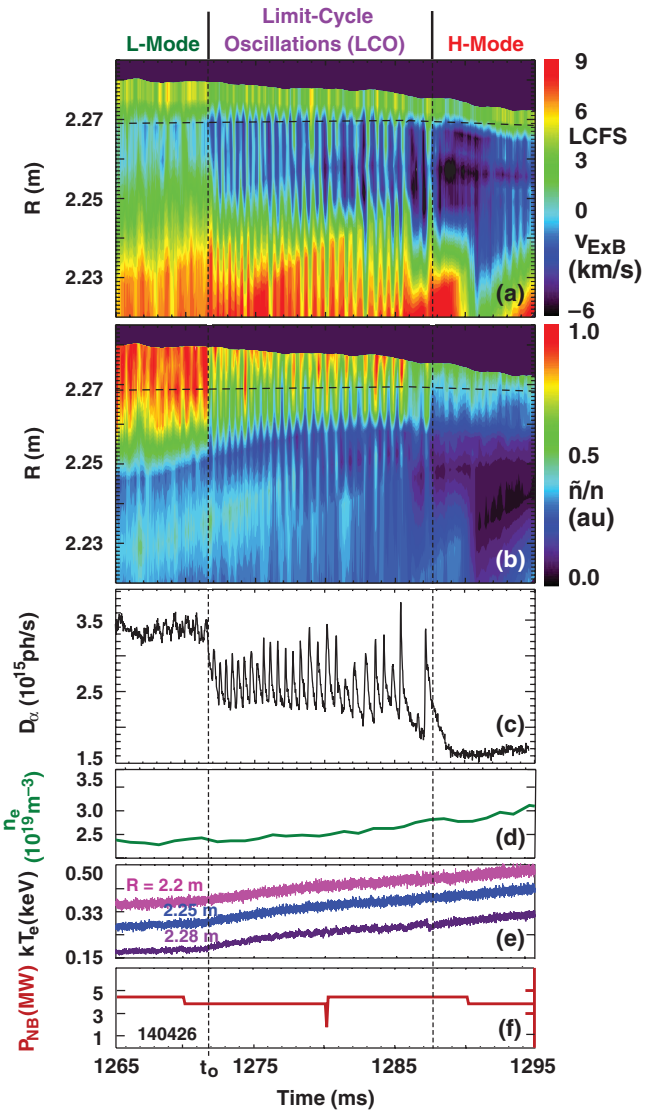

FIG. 1 (color). Time evolution of (a) $\boldsymbol{E} \times \boldsymbol{B}$ velocity (the direction of the ion diamagnetic and ∇B drift is indicated); (b) relative density fluctuation level; (c) divertor D_α signal; (d) electron density; (e) edge electron temperature, and (f) neutral beam power across the transition from L mode through limit cycle oscillations (LCO) to H mode.

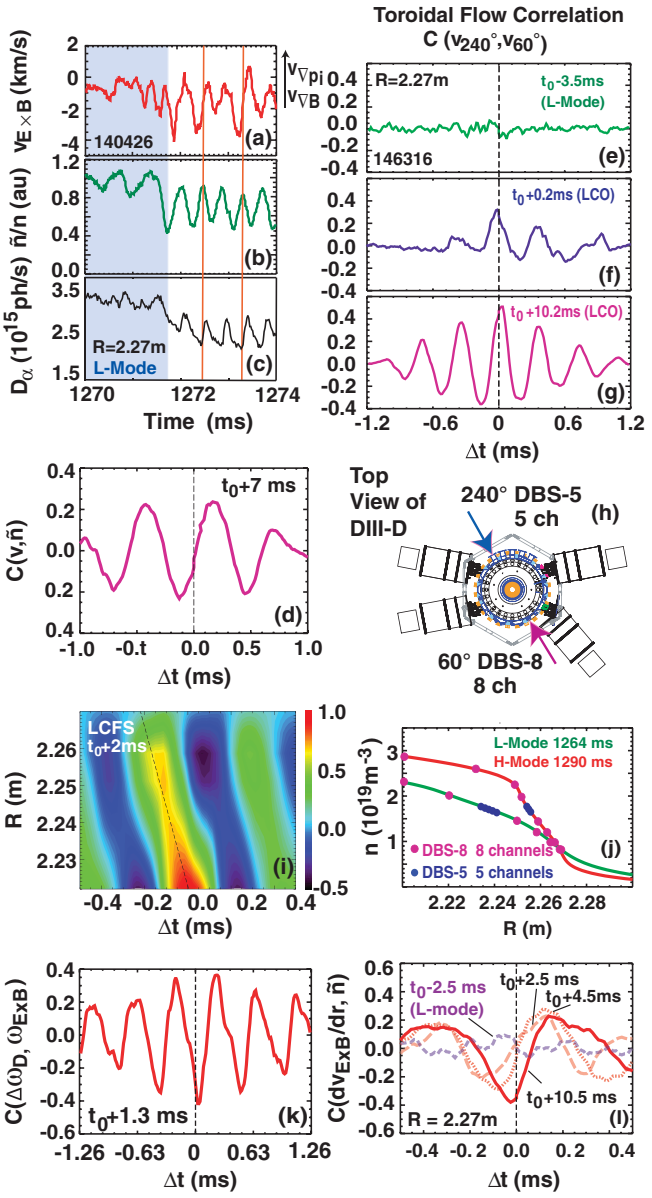

FIG. 2 (color). (a) $\boldsymbol{E}\times\boldsymbol{B}$ velocity; (b) relative density fluctuation level; (c) D_α signal across the onset of predator-prey oscillations; (d) cross-correlation coefficient between $\boldsymbol{E}\times\boldsymbol{B}$ velocity and density fluctuation level; (e–g) toroidal cross-correlation coefficient of $\boldsymbol{E}\times\boldsymbol{B}$ flow; (h) DBS launching locations; (i) velocity cross-correlation coefficient of DBS channels 1-4 with respect to channel 5 used as reference channel (probing a radius $R_1 = 2.245$ m); (j) DBS probing locations in L- and H-mode; (k) cross-correlation of $\Delta\omega_D$ and $\boldsymbol{E}\times\boldsymbol{B}$ shearing rate; (l) cross-correlation coefficient between flow shear and density fluctuation level.

Toroidal/poloidal symmetry of the observed flow oscillation has been explicitly confirmed by cross-correlating the instantaneous Doppler shift between two DBS channels with the same launch frequency ($f = 67.5$ GHz) but displaced 180° toroidally [Fig. 2(h)]. Figures 2(e)–2(g) show that toroidal flow correlation increases substantially at the start of the oscillatory phase ($t = t_0$), consistent with the formation of a low frequency zonal flow.

Figure 2(g) shows that the correlation coefficient $C(v_{240°,60°})$ peaks around zero time lag, confirming the axisymmetric ($k_\Phi = 0$, $k_\theta = 0$) nature of the oscillating flow feature. The zonal flow nature of the limit cycle oscillation (LCO), including the phase relationship between $\tilde{n}$ and $v_{E\times B}$, has been confirmed in several discharges with LCO phases lasting between 5 ms and 400 ms. The observed ZF frequency is much below the expected local GAM frequency $f_{\mathrm{GAM}} = \alpha[(kT_e + (7/4)kT_i)/m_i]^{1/2}/2\pi R \sim 20$ kHz, where α is a numerical factor depending on the plasma shape. The GAM, observed earlier during L mode in the same discharge, typically decreases in amplitude before the L-H transition [9].

Inside the separatrix, radial inward propagation of the ZF with a phase velocity $v_r \sim -220 \pm 40$ m/s, at $t = t_0 +$ 2 ms, has been inferred from the phase of the radial cross-correlation coefficient of the DBS signals, with respect to a reference channel probing $R_1 = 2.245$ m (at toroidal angle $\phi = 60°$ [Fig. 2(i)]). From the instantaneous phase delay a radial wavenumber $k_r \sim -0.7$ cm^{-1} is determined. Inward propagation occurs within one LCO cycle.

Direct evidence of turbulence suppression by Zonal Flow shear has been obtained by comparing the flow shearing rate near the separatrix to the local decorrelation rate $\Delta\omega_D$ of density fluctuations [Fig. 3(a)], derived from the turbulence autocorrelation time τ_{AC} of the DBS scattered signal amplitude (the $1/e$ width of the autocorrelation function), using an analysis window of 40μs. With $\boldsymbol{E}\times\boldsymbol{B}$ advection present, the turbulence decorrelation rate measured in the lab frame is $\Delta\omega_D^{\mathrm{lab}} = \Delta\omega_D(v_{E\times B}/l_\theta)[\Delta\omega_D^{-2} + l_\theta^2/v_{E\times B}^2]^{1/2}$. In the case considered here, $\Delta\omega_D \sim 1/\tau_{\mathrm{AC}} \sim 5\times10^5$ s^{-1} at the separatrix in L-mode in the absence of significant advection ($v_{E\times B} \approx 0$). The measured radial correlation length within the flow layer, $l_r \sim 1$ cm does not change appreciably across the L-mode/limit cycle transition but reduces by ~45% during the final H-mode transition. Estimating the poloidal correlation length as $l_\theta \sim 2l_r$, we find $\Delta\omega_D^{-1} < l_\theta/v_{E\times B}$ except near maximum $\boldsymbol{E}\times\boldsymbol{B}$ flow, and to good approximation $\Delta\omega_D^{\mathrm{lab}} \sim \Delta\omega_D$. Figure 3(a) shows that the initial turbulence suppression results from a fast reduction in the ambient turbulence decorrelation rate (within 100 μs) and a gradual increase in the shearing rate $\omega_{E\times B} = \partial v_{E\times B}/\partial r$. Possible causes for the reduction of $\Delta\omega_D$ may be a reduced eddy turnover time in the shear flow layer (increasing eddy resilience) or an increase in poloidal turbulence correlation length as the ZF is excited. As the Zonal Flow LCO develops, the shearing rate $\omega_{E\times B}$ (measured across the separatrix at $R =$ 2.27 m) periodically exceeds $\Delta\omega_D$ at times coinciding with reduced density fluctuation level [Fig. 3(b)]. The total statistical and systematic errors are estimated to be ±28% on the shearing rate and ±11% on the decorrelation rate (rising to ±16% near maximum $E\times B$ flow), hence

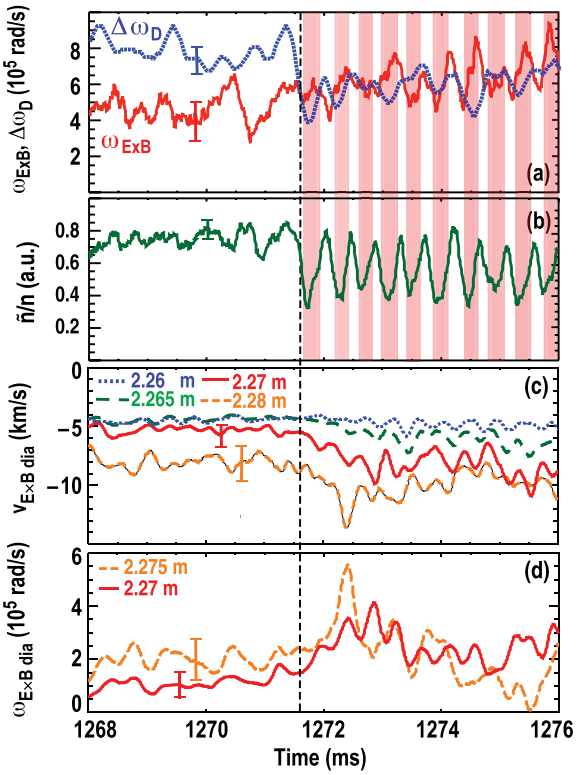

FIG. 3 (color online). (a) Turbulence decorrelation rate and shearing rate across the transition to predator-prey oscillations ($R = 2.27$ m); shading indicates times of turbulence suppression; b) density fluctuation level; (c) diamagnetic component of the $\boldsymbol{E} \times \boldsymbol{B}$ velocity; (d) shearing rate due to the diamagnetic component.

phase-lock averaging the data with respect to the LCO has been employed to reduce the statistical error and confirm that $\omega_{E\times B}$ exceeds $\Delta\omega_D$ at the times when fluctuations are reduced. Also, anticorrelation between decorrelation rate and shearing rate has been systematically confirmed throughout the LCO. The correlation coefficient 1.3 ms after LCO onset is shown in Fig. 2(k).

Figure 3(c) shows the $\boldsymbol{E} \times \boldsymbol{B}$ velocity component due to the ion main pressure gradient, estimated from the electron density profile (a good approximation as $Z_{\rm eff}(R = R_{\rm sep}) < 1.6$ and the local impurity (carbon) ion density $n_C < 0.02 n_e$, hence $n_i \sim n_e$) and the carbon ion temperature profile (from CER, a good approximation due to the high ion collisionality). It is obvious that the pressure gradient begins to increase *after* the $\boldsymbol{E} \times \boldsymbol{B}$ shearing rate exceeds the turbulence decorrelation rate at $t \sim 1271.6$ ms. Comparing the shear due to the diamagnetic component of the $\boldsymbol{E} \times \boldsymbol{B}$ velocity [Fig. 3(d)] to the total $\boldsymbol{E} \times \boldsymbol{B}$ shear measured by DBS [Fig. 3(a)] it is clear that the former increases with pressure profile evolution after the initial turbulence suppression and *after* the start of the predator-prey oscillation. From total $\boldsymbol{E} \times \boldsymbol{B}$ flow measured by DBS we estimate that equilibrium shear due to the main ion $\boldsymbol{v_i} \times \boldsymbol{B}$ component (not measured) accounts for half of the

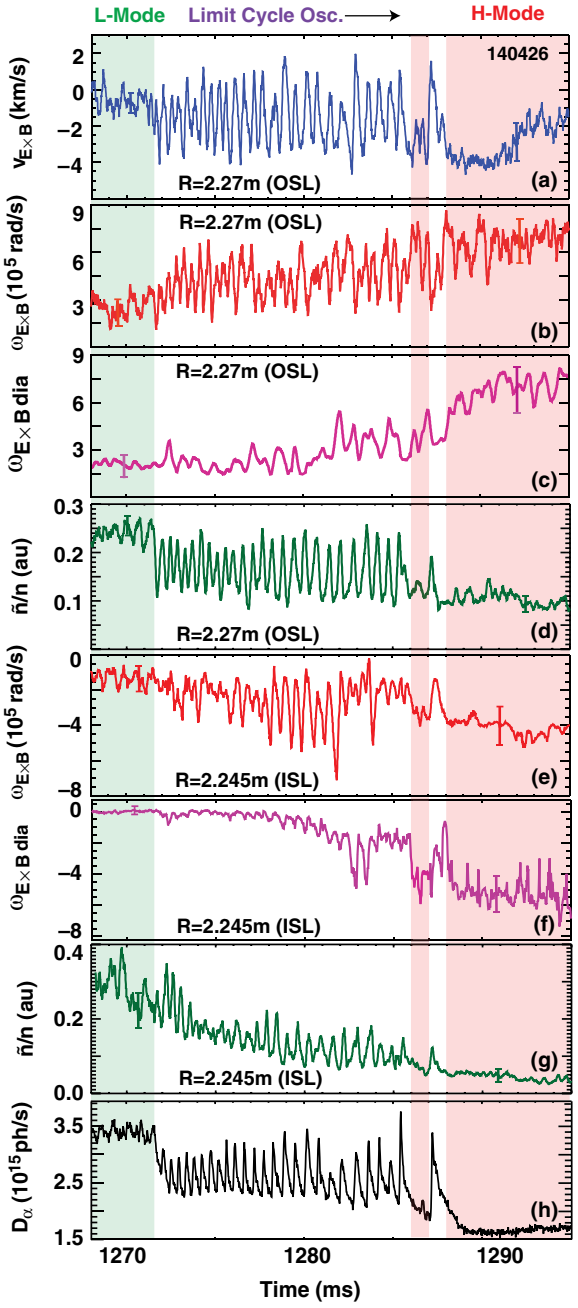

FIG. 4 (color online). (a) $\boldsymbol{E} \times \boldsymbol{B}$ velocity; (b) total $\boldsymbol{E} \times \boldsymbol{B}$ shearing rate; (c) diamagnetic component of $\boldsymbol{E} \times \boldsymbol{B}$ shearing rate; (d) density fluctuation level $\tilde{n}/n$ in the outer shear layer (OSL); (e) total $\boldsymbol{E} \times \boldsymbol{B}$ shearing rate, (f) diamagnetic shearing rate; (g) fluctuation level in the inner shear layer (ISL). For reference, the D_α recycling light signal is shown in (h).

L-mode shear and increases gradually during the predator-prey phase. However, the initial periodic turbulence suppression is clearly linked to the oscillating (ZF) shear.

The time evolution of $\boldsymbol{E} \times \boldsymbol{B}$ velocity, flow shear, and normalized turbulence level throughout the predator-prey phase and the final transition to sustained H mode is shown in Fig. 4. The electric field time evolution shown in

Fig. 4(a) (confirmed by additional plasma shots analyzed) justifies neglecting the turbulence phase velocity compared to the $\boldsymbol{E} \times \boldsymbol{B}$ velocity as the there is no indication of a systematic change of slope near $E_r = 0$ (expected if the turbulence phase velocity would be sizeable). Periodic increases in flow shear occur throughout the predator-prey phase in both the outer shear layer spanning the separatrix [the outboard edge of the electric field well shown in Fig. 1(a)] and the inner shear layer (the inboard edge of the electric field well, 2.23 m $\leq R \leq$ 2.26 m). The oscillatory ZF shear in the outer shear layer dominates initially [Fig. 4(b)]. The shear in the inner layer increases $\sim$1.5 ms after ZF onset [Fig. 4(e)]. Fluctuations in the inner layer exhibit limit cycle oscillations but are gradually substantially reduced [Fig. 4(g)].

The reduced fluctuation level (and radial transport) in time allows the pressure gradient and the equilibrium diamagnetic shear to increase substantially in both layers [Figs. 4(c) and 4(f)]. The predator-prey cycle lengthens as the fluctuation level recovers more slowly after each ZF-induced quench, due to the additional equilibrium shear. This is consistent with the competition between ZF and equilibrium (mean) flow shear advocated in the theoretical predator-prey model [11], where the mean flow shear has been predicted to inhibit ZF growth. The final transition to sustained H mode at $t \sim 1288$ ms is preceded by a transient H-mode phase at 1286–1287 ms. The increase in equilibrium shear maintains fluctuation reduction longer than in previous predator-prey cycles even though the ZF shear decreases in time. Density fluctuations eventually return transiently, in turn again increasing the ZF amplitude and ZF shear. However, after the next quench the pressure gradient and equilibrium shear are sufficient for sustained turbulence suppression; the final H-mode transition has occurred [Fig. 4(h)]. At the time of the final H-mode transition, the diamagnetic shear accounts approximately for the entire measured equilibrium $\boldsymbol{E} \times \boldsymbol{B}$ shear.

The importance of the interplay between ZF and equilibrium shear is reflected in a fundamental change of the cross-correlation between flow shear and turbulence amplitude [Fig. 2(l)]. In L-mode, flow shear is weak, and there is no measurable cross-correlation (shown here for the outer shear layer, $R = 2.27$ m). For $t > t_0$, the flow shear lags $\tilde{n}/n$ by $\sim$90° consistent with the predator-prey model. However, when the equilibrium shear becomes important, the phase lag moves towards 180° (anticorrelation). This phase relationship results from periodic increase or decrease of the edge pressure gradient: as $\tilde{n}/n$ and edge transport increase, ∇p_i flattens, reducing the equilibrium shear. Hence a phase lag near 180° is a strong indication that equilibrium shear suppression has become dominant. Detailed modeling of the interaction between equilibrium or oscillating shear flow and turbulence properties, with inclusion of radial transport and radial profile effects (1-D model), will likely be required for a quantitative comparison of experiment and theory, as described in [19] for externally imposed equilibrium and oscillating $\boldsymbol{E} \times \boldsymbol{B}$ flow shear.

In conclusion we have provided strong experimental evidence that ZF and equilibrium shear are instrumental in the L-H transition, supporting the two-predator–one prey transition model [11]. ZF generation and the resulting strong oscillating shear in the outer shear layer (spanning the separatrix) are crucial in initial turbulence suppression. Increasing ZF shear in the outer and inner shear layer then allow the edge pressure gradient to increase. The shear associated with the diamagnetic component of the $\boldsymbol{E} \times \boldsymbol{B}$ velocity eventually lengthens the predator-prey oscillation cycle until equilibrium shear is sufficient to maintain continuous turbulence suppression consistent with H-mode confinement.

This work is supported by the U. S. Department of Energy under DE-FG02-08ER54984, DE-FG03-01ER54615 and DE-FC02-04ER54698.

[1] F. H. Busse, Chaos **4**, 123 (1994).
[2] P. H. Diamond, S-I. Itoh, K. Itoh, and T. Hahm, Plasma Phys. Controlled Fusion **47**, R35 (2005).
[3] A. Fujisawa, Nucl. Fusion **49**, 013001 (2009).
[4] F. Wagner *et al.*, Phys. Rev. Lett. **49**, 1408 (1982).
[5] R. Groebner, K. H. Burrell, and R. P. Seraydarian, Phys. Rev. Lett. **64**, 3015 (1990).
[6] P. Gohil, T. C. Jernigan, T. H. Osborne, J. T. Scoville, and E. J. Strait, Nucl. Fusion **50**, 064011 (2010).
[7] R. Moyer, G. R. Tynan, C. Holland, and M. J. Burin, Phys. Rev. Lett. **87**, 135001 (2001).
[8] R. J. Colchin *et al.*, Phys. Rev. Lett. **88**, 255002 (2002).
[9] G. R. McKee *et al.*, Nucl. Fusion **49**, 115016 (2009).
[10] T. Estrada *et al.*, Plasma Phys. Controlled Fusion **51**, 124015 (2009).
[11] E. J. Kim and P. H. Diamond, Phys. Rev. Lett. **90**, 185006 (2003).
[12] S. J. Zweben, R. J. Maqueda, R. Hager, K. Hallatschek, S. M. Kaye, T. Munsat, F. M. Poli, A. L. Roquemore, Y. Sechrest, and D. P. Stotler, Phys. Plasmas **17**, 102502 (2010).
[13] G. D. Conway, C. Angioni, F. Ryter, P. Sauter, J. Vicente, and ASDEX Upgrade Team, Phys. Rev. Lett. **106**, 065001 (2011).
[14] G. S. Xu *et al.*, Phys. Rev. Lett. **107**, 125001 (2011).
[15] Y. H. Xu, C. X. Yu, J. R. Luo, J. S. Mao, B. H. Liu, J. G. Li, B. N. Wan, and Y. X. Wan, Phys. Rev. Lett. **84**, 3867 (2000).
[16] J. C. Hillesheim, W. A. Peebles, T. L. Rhodes, L. Schmitz, A. E. White, and T. A. Carter, Rev. Sci. Instrum. **81**, 10D907 (2010).
[17] W.A.Peebles, T.L. Rhodes, J.C. Hillesheim, L. Zeng, and C. Wannberg, Rev. Sci. Instrum. **81**, 10D902 (2010).
[18] G. D. Conway *et al.*, *Proc. 8th Int. Reflectometry Workshop* (St Petersburg, Russia (2007), http://www.aug.ipp.mpg.de/IRW/IRW8
[19] Maeyama, A. Ishizawa, T.-H. Watanabe, M. M. Škorić, N. Nakajima, S. Tsuji-Iio, and H. Tsutsui, Phys. Plasmas **17**, 062305 (2010).